

Jellium at finite temperature

Riccardo Fantoni^{1,*}

¹*Università di Trieste, Dipartimento di Fisica,
strada Costiera 11, 34151 Grignano (Trieste), Italy*

(Dated: October 15, 2021)

arXiv:2110.07527v1 [cond-mat.str-el] 14 Oct 2021

Abstract

We adopt the fixed node restricted path integral Monte Carlo method within the “Worm algorithm” to simulate Wigner’s Jellium model at finite, non zero, temperatures using free-particle nodes of the density matrix. The new element is that we incorporate the Worm algorithm paradigm of Prokof’ev and Svistunov in the grand canonical ensemble in order to more efficiently handle the fermionic exchanges. We present results for the structure and thermodynamic properties of the ideal Fermi gas and three points for the interacting electron gas. We treat explicitly the case of the partially polarized electron gas.

PACS numbers: 02.70.Ss,05.10.Ln,05.30.Fk,05.70.-a,61.20.Ja,61.20.Ne

Keywords: Jellium, Monte Carlo simulation, finite temperature, path integral, worm algorithm, restricted path integral, fermions sign problem, structure, thermodynamic properties

I. INTRODUCTION

The free electron gas or the *Jellium* model of Wigner [1, 2] is the simplest physical model for the valence electrons in a metal [3] (more generally it is an essential ingredient for the study of ionic liquids (see Ref. [4] Chapter 10 and 11): molten-salts, liquid-metals, and ionic-solutions) or the plasma in the interior of a white dwarf [5]. It can be imagined as a system of pointwise electrons of charge e made thermodynamically stable by the presence of a uniform inert neutralizing background of opposite charge density inside which they move. In this work we will only be interested in the jellium in the three dimensional Euclidean space, leaving its study in a curved surface [6–9] to later studies.

The zero temperature, ground-state, properties of the statistical mechanical system thus depends just on the electronic density n , or the Wigner-Seitz radius $r_s = (3/4\pi n)^{1/3}/a_0$ where a_0 is Bohr radius, or the Coulomb coupling parameter $\Gamma = e^2/(a_0 r_s)$. Free electrons in metallic elements [3] has $2 \lesssim r_s \lesssim 4$ whereas in the interior of a white dwarf [5] $r_s \simeq 0.01$.

The recent two decades have witnessed an impressive progress in experiments and also in quantum Monte Carlo simulations which have provided the field with the most accurate thermodynamic data available. These simulations started with the work by Ceperley

* rfantoni@ts.infn.it

and co-workers and Filinov and co-workers for jellium [10–18], hydrogen, hydrogen-helium mixtures and electron-hole plasmas in the 1990s and have been improved dramatically. We recently also applied our newly developed method to the binary fermion-boson plasma mixture at finite temperature [19], where we discussed the thermodynamic stability of the two component mixture where the two species are both bosons, both fermions, and one boson and one fermion.

According to Lindhard theory of static screening, [20] suppose we switch on an appropriately screened test charge potential δV in a free electron gas. The Hartree potential $\delta V(\mathbf{r})$ created at a distance r from a static point charge of magnitude e at the origin, should be evaluated self-consistently from the Poisson equation,

$$\nabla^2 \delta V(\mathbf{r}) = -4\pi e^2 [\delta(\mathbf{r}) + \delta n(\mathbf{r})] \quad , \quad (1.1)$$

where $\delta n(\mathbf{r})$ is the change in electronic density induced by the test charge. The electron density $n(\mathbf{r})$ may be written as

$$n(\mathbf{r}) = 2 \sum_{\mathbf{k}} |\psi_{\mathbf{k}}(\mathbf{r})|^2 \quad , \quad (1.2)$$

where $\psi_{\mathbf{k}}(\mathbf{r})$ are single-electron orbitals, the sum over \mathbf{k} is restricted to occupied orbitals ($|\mathbf{k}| \leq k_F$, where k_F is the Fermi wave vector) and the factor 2 comes from the sum over spin orientations. We must now calculate how the orbitals in the presence of the test charge, differ from plane waves $\exp(i\mathbf{k} \cdot \mathbf{r})$. We use for this purpose the Schrödinger equation,

$$\nabla^2 \psi_{\mathbf{k}}(\mathbf{r}) + \left[k^2 - \frac{2m}{\hbar^2} \delta V(r) \right] \psi_{\mathbf{k}}(\mathbf{r}) = 0 \quad , \quad (1.3)$$

having imposed that the orbitals reduce to plane waves with energy $\hbar^2 k^2 / (2m)$ at large distance ¹.

With the aforementioned boundary condition the Schrödinger equation may be converted into an integral equation,

$$\psi_{\mathbf{k}}(\mathbf{r}) = \frac{1}{\sqrt{\Omega}} e^{i\mathbf{k} \cdot \mathbf{r}} + \frac{2m}{\hbar^2} \int G_{\mathbf{k}}(\mathbf{r} - \mathbf{r}') \delta V(\mathbf{r}') \psi_{\mathbf{k}}(\mathbf{r}') d\mathbf{r}' \quad , \quad (1.4)$$

with $G_{\mathbf{k}}(\mathbf{r}) = -\exp(i\mathbf{k} \cdot \mathbf{r}) / (4\pi r)$ and Ω the volume of the system.

¹ This approach (which lead to the Random Phase Approximation, RPA) is approximate insofar as the potential entering the Schrödinger equation has been taken as the Hartree potential, thus neglecting exchange and correlation between an incoming electron and the electronic screening cloud.

Within linear response theory we can replace $\psi_{\mathbf{k}}(\mathbf{r})$ by $\Omega^{-1/2} \exp(i\mathbf{k} \cdot \mathbf{r})$ inside the integral. This yields

$$\delta n(\mathbf{r}) = -\frac{mk_F^2}{2\pi^3\hbar^2} \int j_1(2k_F|\mathbf{r} - \mathbf{r}'|) \frac{\delta V(\mathbf{r}')}{|\mathbf{r} - \mathbf{r}'|^2} d\mathbf{r}' \quad , \quad (1.5)$$

with $j_1(x)$ being the first-order spherical Bessel function $[\sin(x) - x \cos(x)]/x^2$. Using this result in the Poisson equation we get

$$\nabla^2 \delta V(r) = -4\pi e^2 \delta(\mathbf{r}) + \frac{2mk_F^2 e^2}{\pi^2 \hbar^2} \int j_1(2k_F|\mathbf{r} - \mathbf{r}'|) \frac{\delta V(\mathbf{r}')}{|\mathbf{r} - \mathbf{r}'|^2} d\mathbf{r}' \quad , \quad (1.6)$$

which is easily soluble in Fourier transform. Writing $\delta V(k) = 4\pi e^2/[k^2 \varepsilon(k)]$ we find,

$$\varepsilon(k) = 1 + \frac{2mk_F e^2}{\pi k^2 \hbar^2} \left[1 + \frac{k_F}{k} \left(\frac{k^2}{4k_F^2} - 1 \right) \ln \left| \frac{k - 2k_F}{k + 2k_F} \right| \right] \quad , \quad (1.7)$$

which is the static dielectric function in RPA.

For $k \rightarrow 0$ this expression gives $\varepsilon(k) \rightarrow 1 + k_{TF}^2/k^2$ with $k_{TF} = 3\omega_p^2/v_F^2$ (ω_p being the plasma frequency and v_F the Fermi velocity) i.e. the result of the Thomas-Fermi theory. However $\varepsilon(k)$ has a singularity at $k = \pm 2k_F$, where its derivative diverges logarithmically². This singularity in $\delta V(k)$ determines, after Fourier transform, the behavior of $\delta V(r)$ at large r . $\delta V(r)$ turns out to be an oscillating function [21] rather than a monotonically decreasing function as in the Thomas-Fermi theory. Indeed,

$$\delta V(r) = \int \frac{d\mathbf{k}}{(2\pi)^3} \frac{4\pi e^2}{k^2 \varepsilon(k)} e^{i\mathbf{k} \cdot \mathbf{r}} = \frac{e^2}{i\pi r} \int_{-\infty}^{\infty} dk \frac{e^{ikr}}{k \varepsilon(k)} \quad , \quad (1.8)$$

and the integrand has non-analytic behavior at $q = \pm 2k_F$,

$$\left[\frac{1}{k \varepsilon(k)} \right]_{k \rightarrow \pm 2k_F} = -A(k - (\pm)2k_F) \ln |k - (\pm)2k_F| + \text{regular terms} \quad , \quad (1.9)$$

with $A = (k_{TF}^2/4k_F^2)/(k_{TF}^2 + 8k_F^2)$. Hence,

$$\begin{aligned} \delta V(r)|_{r \rightarrow \infty} &= -\frac{Ae^2}{i\pi r} \int_{-\infty}^{\infty} dk e^{ikr} [(k - 2k_F) \ln |k - 2k_F| \\ &\quad + (k + 2k_F) \ln |k + 2k_F|] = -2Ae^2 \frac{\cos(2k_F r)}{r^3} \quad . \end{aligned} \quad (1.10)$$

This result is based on a theorem on Fourier transforms, [22] stating that the asymptotic behavior of $\delta V(r)$ is determined by the low- k behavior as well as the singularities of $\delta V(k)$. Obviously, in the present case the asymptotic contribution from the singularities is dominant

² The discontinuity in the momentum distribution across the Fermi surface introduces a singularity in elastic scattering processes with momentum transfer equal to $2k_F$.

over the exponential decay of Thomas-Fermi type. The result implies that the screened ion-ion interaction in a metal has oscillatory character and ranges over several shells of neighbors.

Today we are able to simulate on a computer the structural and thermodynamic properties of Jellium at finite, non zero, temperature. This allows us to predict thermodynamic states that would be rather difficult to obtain in nature or in the laboratory. Such as Jellium under extreme conditions, partially polarized Jellium, etc.. In this work we will carry on some of these path integral simulations which make use of the Monte Carlo technique, which is the best known method to compute a path integral. [23] The *computer experiment* is alternative to the theoretical analytical approximations like RPA that has been developed, during the years, with various degrees of accuracies in different thermodynamic conditions. Such theoretical approximations generally fall into two categories: those which extend down from the classical regime and those which assume some interpolation between the $T = 0$ and high- T regimes. From the former group we recall the Debye-Hückel (DH) theory which solves for the Poisson-Boltzmann equations for the classical one-component plasma and the quantum corrections of Hansen *et al.* [24, 25] of the Coulomb system both with Wigner-Kirkwood corrections (H+WK) and without (H). Clearly these methods do not perform well in the quantum regime below the Fermi temperature since they lack quantum exchange. The Random Phase Approximation (RPA) [26, 27] is a reasonable approximation in the low-density, high-temperature limit (where it reduces to DH) and the low-temperature, high-density limit, since these are both weakly interacting regimes. Its failure, however, is most apparent in its estimation of the equilibrium, radial distribution function $g(r)$ which becomes negative for stronger coupling. Extensions of the RPA into intermediate densities and temperatures have largely focused on constructing local-field corrections (LFC) through interpolation since diagrammatic resummation techniques often become intractable in strongly-coupled regimes. Singwi *et al.* [28] introduced one such strategy. Tanaka and Ichimaru [29] (TI) extended this method to finite temperatures and provided the parameterization of the Jellium correlation energy. This method appear to perform marginally better than the RPA at all temperatures, though it still fails to produce a positive-definite $g(r)$ at values of $r_s > 2$. A third, more recent approach introduced by Perrot and Dharma-wardana (PDW) [30] relies on a classical mapping where the distribution functions of a classical system at temperature T_{cf} , solved for through the hypernetted-chain equation, reproduce those for the quantum system at temperature T . In a previous work, PDW showed such a temper-

ature T_q existed for the classical system to reproduce the correlation energy of the quantum system at $T = 0$. [31] To extend this work to finite temperature quantum systems, they use the simple interpolation formula $T_{cf} = \sqrt{T^2 + T_q^2}$. This interpolation is clearly valid in the low- T limit where Fermi liquid theory gives the quadratic dependence of the energy on T . Further in the high- T regime, T dominates over T_q as the system becomes increasingly classical. The PDW results matches well with the simulation results in these two limits. It is not surprising, however, that in the intermediate temperature regime, where correlation effects are greatest, the quadratic interpolation fails. A contemporary, but similar approach by Dutta and Dufty [32] uses the same classical mapping as PDW which relies on matching the $T = 0$ pair correlation function instead of the correlation energy. While we expect this to give more accurate results near $T = 0$, we would still expect a breakdown of the assumed Fermi liquid behavior near the Fermi temperature. Strict benchmarks have only recently been presented in Ref. [33]. Future Jellium work will include creating a new parameterization of the exchange-correlation energy which uses the simulation data directly. [16, 34, 35] In doing so, simulations at higher densities and both lower and higher temperatures may be necessary in order to complete the interpolation between the ground-state and classical limits.

As will be made clear in Section IV, till recently, not even through computer experiments we were able to obtain exact numerical results, since one had to face the so called *fermions sign problem* which had not been solved before the advent of recent simulation [15, 16] when it was demonstrated that the fermion sign problem can be completely avoided and exact results (with an error below 1%) for the thermodynamic functions can be obtained. In other words we were not able to extract exact results not even numerically from a simulation for fermions, unlike for bosons or boltzmannons. Therefore, in order to circumvent the fermion sign problem, we will here resort to the most widely used approximation in quantum Monte Carlo that is the *restricted path integral* fixed nodes method. [36, 37] But unlike previous studies we will implement this method upon the *worm* algorithm [38, 39] in the grand canonical ensemble. This complements our previous study [2] carried out in the canonical ensemble. In this work we will be just interested in proving the validity of our new numerical scheme but not his accuracy. We will then not worry about the finite size corrections, the imaginary thermal time discretization error, and about a stringent comparison with previous canonical ensemble studies available in literature since this program has been already carried

on in Ref. [2].

The work is organized as follows: in Section II we describe the Jellium model from a physical point of view, in Section III we introduce the parameter space necessary for the description of Jellium at finite temperature, in Section IV we describe the simulation method, in Section V we outline the problem we want to solve on a computer, in Section VI we presents some details of our new algorithm, Section VII is for our numerical results, and in Section VIII we summarize our concluding remarks.

II. THE MODEL

The *Jellium* model of Wigner [20, 40–42] is an assembly of N_+ spin up pointwise electrons and N_- spin down pointwise electrons of charge e moving in a positive inert background that ensures charge neutrality. The total number of electrons is $N = N_+ + N_-$ and the average particle number density is $n = N/\Omega$, where Ω is the volume of the electron fluid. In the volume $\Omega = L^3$ there is a uniform neutralizing background with a charge density $\rho_b = -en$. So that the total charge of the system is zero. The fluid polarization is then $\xi = |N_+ - N_-|/N$: $\xi = 0$ in the unpolarized (paramagnetic) case and $\xi = 1$ in the fully polarized (ferromagnetic) case.

Setting lengths in units of $a = (4\pi n/3)^{-1/3}$ and energies in Rydberg's units, $\text{Ry} = \hbar^2/2ma_0^2$, where m is the electron mass and $a_0 = \hbar^2/me^2$ is the Bohr radius, the Hamiltonian of Jellium is

$$\mathcal{H} = -\frac{1}{r_s^2} \sum_{i=1}^N \nabla_{\mathbf{r}_i}^2 + V(R), \quad (2.1)$$

$$V = \frac{1}{r_s} \left(2 \sum_{i<j} \frac{1}{|\mathbf{r}_i - \mathbf{r}_j|} + \sum_{i=1}^N r_i^2 + v_0 \right), \quad (2.2)$$

where $R = (\mathbf{r}_1, \mathbf{r}_2, \dots, \mathbf{r}_N)$ with \mathbf{r}_i the coordinate of the i th electron, $r_s = a/a_0$, and v_0 a constant containing the self energy of the background. Note that the presence of the neutralizing background produces the harmonic confinement shown in Eq. (2.2).

The kinetic energy scales as $1/r_s^2$ and the potential energy (particle-particle, particle-background, and background-background interaction) scales as $1/r_s$, so for small r_s (high electronic densities), the kinetic energy dominates and the electrons behave like an ideal gas. In the limit of large r_s , the potential energy dominates and the electrons crystallize into a

Wigner crystal. [43] No liquid phase is realizable within this model since the pair-potential has no attractive parts even though a superconducting state [44] may still be possible (see chapter 8.9 of Ref. [45] and Ref. [46]).

The Jellium has been solved either by integral equation theories in its ground-state [28] or by computer experiments in its ground-state [47] in the second half of last century but more recently it has been studied at finite, non zero, temperatures by several research groups. [10–12, 14–18]

It was shown in Ref. [13] that the data of Brown *et al.* [10, 11] are inaccurate at $r_s = 1$. This appears to be a systematic error of the fixed node method so it would be interesting to know whether this problem may be solved with the present method which seems a promising route to access higher densities which was not possible in the paper by Brown *et al.*

III. JELLIUM AT FINITE TEMPERATURE

For the Jellium at finite temperature it is convenient to introduce the *electron degeneracy parameter* $\Theta = T/T_F$, where T_F is the Fermi temperature

$$T_F = T_D \frac{(2\pi)^2}{2[(2 - \xi)\alpha_3]^{2/3}}, \quad (3.1)$$

here ξ is the polarization of the fluid that can be either $\xi = 0$, for the unpolarized case, and $\xi = 1$, for the fully polarized case, $\alpha_3 = 4\pi/3$, and

$$T_D = \frac{n^{2/3}\hbar^2}{mk_B} = \frac{\hbar^2}{mk_B\alpha_3^{2/3}(a_0r_s)^2}, \quad (3.2)$$

is the degeneracy temperature, [23] for temperatures higher than T_D quantum effects are less relevant.

The state of the fluid will then depend also upon the *Coulomb coupling parameter*, $\Gamma = e^2/(a_0r_s)k_B T$. [10] So that

$$\Theta = \frac{r_s}{\Gamma} \left[\frac{2(2 - \xi)^{2/3}\alpha_3^{4/3}}{(2\pi)^2} \right]. \quad (3.3)$$

The behavior of the internal energy of the Jellium in its ground-state ($\Theta = 0$) has been determined through Diffusion Monte Carlo (DMC) by Ceperley and Alder. [47] Three phases of the fluid appeared, for $r_s < 75$ the stable phase is the one of the unpolarized Jellium, for $75 < r_s < 100$ the one of the polarized fluid, and for $r_s > 100$ the one of the Wigner crystal. They used systems from $N = 38$ to $N = 246$ electrons.

IV. THE SIMULATION

The *density matrix* of a system of many fermions at temperature $k_B T = \beta^{-1}$ can be written as an integral over all paths $\{R_t\}$

$$\rho_F(R_\beta, R_0; \beta) = \frac{1}{N!} \sum_{\mathcal{P}} (-1)^{\mathcal{P}} \oint_{\mathcal{P}R_0 \rightarrow R_\beta} dR_t \exp(-S[R_t]). \quad (4.1)$$

the path R_t begins at $\mathcal{P}R_0$ and ends at R_β and \mathcal{P} is a permutation of particles labels. For nonrelativistic particles interacting with a potential $V(R)$ the *action* of the path, $S[R_t]$, is given by (see appendix A)

$$S[R_t] = \int_0^\beta dt \left[\frac{r_s^2}{4} \left| \frac{dR_t}{dt} \right|^2 + V(R_t) \right]. \quad (4.2)$$

Thermodynamic properties, such as the energy, are related to the diagonal part of the density matrix, so that the path returns to its starting place or to a permutation \mathcal{P} after a time β .

To perform Monte Carlo calculations of the integrand, one makes imaginary time discrete with a *time step* τ , so that one has a finite (and hopefully small) number of time slices and thus a classical system of N particles in $M = \beta/\tau$ time slices; an equivalent NM particle classical system of “polymers”. [23]

Note that in addition to sampling the path, the permutation is also sampled. This is equivalent to allowing the ring polymers to connect in different ways. This macroscopic “percolation” of the polymers is directly related to superfluidity as Feynman [48–50] first showed. Any permutation can be broken into cycles. Superfluid behavior can occur at low temperature when the probability of exchange cycles on the order of the system size is non-negligible. The *superfluid fraction* can be computed in a path integral Monte Carlo calculation as described in Ref. [46]. The same method could be used to calculate the *superconducting fraction* in Jellium at low temperature. However, the straightforward application of those techniques to Fermi systems means that odd permutations subtract from the integrand. This is the “fermions sign problem” [36] first noted by Feynman [51] who after describing the path integral theory for boson superfluid ^4He , pointed out: “*The [path integral] expression for Fermi particles, such as ^3He , is also easily written down. However in the case of liquid ^3He , the effect of the potential is very hard to evaluate quantitatively in an accurate manner. The reason for this is that the contribution of a cycle to the sum over permutations is either positive or negative depending whether the cycle has an odd or an even number of atoms in its length L .*”

Thermodynamic properties are averages over the thermal N -fermions density matrix which is defined as a thermal occupation of the exact eigenstates $\phi_i(R)$

$$\rho_F(R, R'; \beta) = \sum_i \phi_i^*(R) e^{-\beta E_i} \phi_i(R'). \quad (4.3)$$

The partition function is the trace of the density matrix

$$Z(\beta) = e^{-\beta F} = \int dR \rho_F(R, R; \beta) = \sum_i e^{-\beta E_i}. \quad (4.4)$$

Other thermodynamic averages are obtained as

$$\langle \mathcal{O} \rangle = Z(\beta)^{-1} \int dR dR' \langle R | \mathcal{O} | R' \rangle \rho_F(R', R; \beta). \quad (4.5)$$

Note that for any density matrix the diagonal part is always positive

$$\rho_F(R, R; \beta) \geq 0, \quad (4.6)$$

so that $Z^{-1} \rho_F(R, R; \beta)$ is a proper probability distribution. It is the diagonal part which we need for many observables, so that probabilistic ways of calculating those observables are, in principle, possible.

Path integrals are constructed using the product property of density matrices

$$\rho_F(R_2, R_0; \beta_1 + \beta_2) = \int dR_1 \rho_F(R_2, R_1; \beta_2) \rho_F(R_1, R_0; \beta_1), \quad (4.7)$$

which holds for any sort of density matrix. If the product property is used M times we can relate the density matrix at a temperature β^{-1} to the density matrix at a temperature $M\beta^{-1}$. The sequence of intermediate points $\{R_1, R_2, \dots, R_{M-1}\}$ is the path, and the *time step* is $\tau = \beta/M$. As the time step gets sufficiently small the Trotter theorem tells us that we can assume that the kinetic \mathcal{T} and potential \mathcal{V} operator commute so that: $e^{-\tau \mathcal{H}} = e^{-\tau \mathcal{T}} e^{-\tau \mathcal{V}}$ and the *primitive approximation* for the fermions density matrix is found. [23] The Feynman-Kac formula for the fermions density matrix results from taking the limit $M \rightarrow \infty$. The price we have to pay for having an explicit expression for the density matrix is additional integrations; all together $3N(M-1)$. Without techniques for multidimensional integration, nothing would have been gained by expanding the density matrix into a path. Fortunately, simulation methods can accurately treat such integrands. It is feasible to make M rather large, say in the hundreds or thousands, and thereby systematically reduce the time-step error.

In addition to the internal energy and the static structure of the Jellium one could also measure its dynamic structure, the “superconducting fraction”, the specific heat, and the pressure. [23]

A. Restricted Path Integral Monte Carlo

In this section we give a brief review of the restricted path integral Monte Carlo (RPIMC) method fully described in Refs. [36, 37]. The fermion density matrix is defined by the Bloch equation which describes its evolution in imaginary time

$$\frac{\partial}{\partial \beta} \rho_F(R, R_0; \beta) = -\mathcal{H} \rho_F(R, R_0; \beta), \quad (4.8)$$

$$\rho_F(R, R_0; 0) = \mathcal{A} \delta(R - R_0), \quad (4.9)$$

where $\beta = 1/k_B T$ with T the absolute temperature and \mathcal{A} is the operator of antisymmetrization. The *reach* of R_0 , $\gamma(R_0, t)$, is the set of points $\{R_i\}$ for which

$$\rho_F(R_{i'}, R_0; t') > 0 \quad 0 \leq t' \leq t, \quad (4.10)$$

where $\hbar t$ is the imaginary thermal time, and is illustrated in Fig. 1. Note that

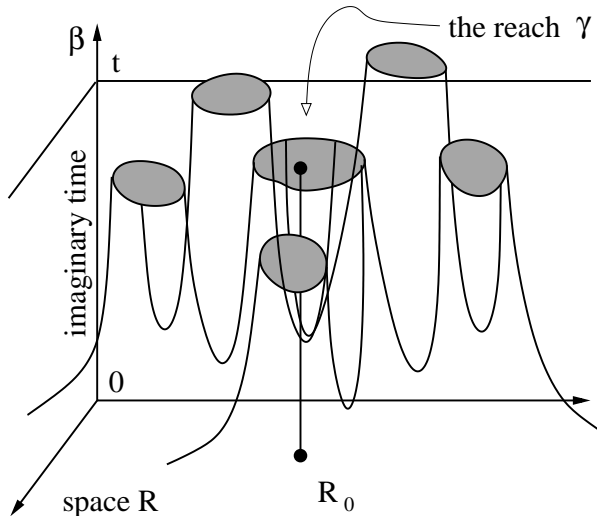


FIG. 1. Illustration of the reach $\gamma(R_0, t)$ of the fermion density matrix.

$$\rho_F(R_0, R_0; t) > 0, \quad (4.11)$$

and clearly

$$\rho_F(R, R_0; t)|_{R \in \partial\gamma(R_0, t)} = 0. \quad (4.12)$$

We want to show that (4.12) uniquely determines the solution. Suppose $\delta(R, t)$ satisfies the Bloch equation

$$\left(\mathcal{H} + \frac{\partial}{\partial t} \right) \delta(R, t) = 0, \quad (4.13)$$

in a space-time domain $\alpha = \{t_1 \leq t \leq t_2, R \in \Omega_t\}$ where Ω_t is the space domain at fixed imaginary thermal time. And the two conditions

$$\delta(R, t_1) = 0, \quad (4.14)$$

$$\delta(R, t)|_{R \in \partial\Omega_t} = 0 \quad t_1 \leq t \leq t_2, \quad (4.15)$$

are also satisfied. Consider

$$\int_{t_1}^{t_2} dt \int_{\Omega_t} dR e^{2V_0 t} \delta(R, t) \left(\mathcal{H} + \frac{\partial}{\partial t} \right) \delta(R, t) = 0, \quad (4.16)$$

where V_0 is a lower bound for $V(R)$.

We have

$$\frac{\partial}{\partial t} [e^{2V_0 t} \delta^2(R, t)] = 2V_0 e^{2V_0 t} \delta^2(R, t) + 2e^{2V_0 t} \delta(R, t) \frac{\partial}{\partial t} \delta(R, t). \quad (4.17)$$

Since

$$\begin{aligned} \int_{t_1}^{t_2} dt \int_{\Omega_t} dR \frac{\partial}{\partial t} \left(\frac{e^{2V_0 t}}{2} \delta^2(R, t) \right) &= \int_{t_1}^{t_2} dt \frac{\partial}{\partial t} \left(\frac{e^{2V_0 t}}{2} \int_{\Omega_t} dR \delta^2(R, t) \right) \\ &= \frac{e^{2V_0 t_2}}{2} \int_{\Omega_{t_2}} dR \delta^2(R, t_2), \end{aligned} \quad (4.18)$$

where in the last equality we used Eq. (4.14). Then from Eq. (4.16) follows

$$\begin{aligned} &\frac{e^{2V_0 t_2}}{2} \int_{\Omega_{t_2}} dR \delta^2(R, t_2) - \\ &\int_{t_1}^{t_2} dt e^{2V_0 t} \int_{\Omega_t} dR [V_0 \delta^2(R, t) - \delta(R, t) \mathcal{H} \delta(R, t)] = 0. \end{aligned} \quad (4.19)$$

Then using Eq. (4.15) we find

$$\begin{aligned} &\frac{e^{2V_0 t_2}}{2} \int_{\Omega_{t_2}} dR \delta^2(R, t_2) + \\ &\int_{t_1}^{t_2} dt e^{2V_0 t} \int_{\Omega_t} dR [(V(R) - V_0) \delta^2(R, t) + \lambda (\nabla \delta(R, t))^2] = 0. \end{aligned} \quad (4.20)$$

With $\lambda = \hbar^2/2m$. Each term in Eq. (4.20) is non-negative so it must be

$$\delta(R, t) = 0 \quad \text{in } \alpha. \quad (4.21)$$

Let ρ_1 and ρ_2 be two solutions of the restricted path problem and let $\delta = \rho_1 - \rho_2$. Then $\delta(R, t)|_{R \in \partial\gamma(R_0, t)} = 0$ for $t_1 \leq t \leq t_2$. By taking t_2 to infinity and t_1 to zero we conclude that the fermion density matrix is the unique solution.

Eq (4.20) also shows that the reach γ has the *tiling* property. [36] Suppose it did not. Then there would exist a space-time domain with the density matrix non-zero inside and from which it is only possible to reach R_0 or any of its images $\mathcal{P}R_0$, with \mathcal{P} any permutation of the particles, crossing the nodes of the density matrix. But such a domain cannot extend to $t = 0$ because in the classical limit there are no nodes. Then this density matrix satisfies for some $t_1 > 0$ the boundary conditions (4.14) and (4.15) and as a consequence it must vanish completely inside the domain contradicting the initial hypothesis.

We now derive the restricted path identity. Suppose ρ_F is the density matrix corresponding to some set of quantum numbers which is obtained by using the projection operator \mathcal{A} on the distinguishable particle density matrix. Then it is a solution to the Bloch equation (4.8) with boundary condition (4.9). Thus we have proved the *Restricted Path Integral* identity

$$\rho_F(R_\beta, R_0; \beta) = \int dR' \rho_F(R', R_0; 0) \oint_{R' \rightarrow R_\beta \in \gamma(R_0)} dR_t e^{-S[R_t]}, \quad (4.22)$$

where the subscript means that we restrict the path integration to paths starting at R' , ending at R_β and node-avoiding. The weight of the walk is $\rho_F(R', R_0; 0) = (N!)^{-1} \sum_{\mathcal{P}} (-)^{\mathcal{P}} \delta(R' - \mathcal{P}R_0)$. It is clear that the contribution of all the paths for a single element of the density matrix will be of the same sign, thus solving the sign problem; positive if $\rho_F(R', R_0; 0) > 0$, negative otherwise. On the diagonal the density matrix is positive and on the path restriction $\rho_F(R, R_0; \beta) > 0$ then only even permutations are allowed since $\rho_F(R, \mathcal{P}R; \beta) = (-)^{\mathcal{P}} \rho_F(R, R; \beta)$. It is then possible to use a bosons calculation to get the fermions case.

Important in this argument is that the random walk is a continuous process so we can say definitely that if sign of the density matrix changed, it had to have crossed the nodes at some point.

The restricted path identity is one solution to Feynman's task of rearranging terms to keep only positive contributing paths for diagonal expectation values.

The problem we now face is that the unknown density matrix appears both on the left-hand side and on the right-hand side of Eq. (4.22) since it is used to define the criterion of node-avoiding paths. To apply the formula directly, we would somehow have to self-consistently determine the density matrix. In practice what we need to do is make an *ansatz*, which we call ρ_T , for the nodes of the density matrix needed for the restriction. The *trial density matrix*, ρ_T , is used to define trial nodal cells: $\gamma_T(R_0)$.

Then if we know the reach of the fermion density matrix we can use the Monte Carlo method to solve the fermion problem restricting the path integral (RPIMC) to the space-time domain where the density matrix has a definite sign (this can be done, for example, using a trial density matrix whose nodes approximate well the ones of the true density matrix) and then using the antisymmetrization operator to extend it to the whole configuration space. This will require the complicated task of sampling the permutation space of the N -particles. [23] Recently it has been devised an intelligent method to perform this sampling through a new algorithm called the *worm* algorithm. [38, 39] In order to sample the path in coordinate space one generally uses various generalizations of the Metropolis rejection algorithm [52] and the *bisection method* [23] in order to accomplish multislice moves which becomes necessary as τ decreases.

The *pair-product approximation* was used by Brown *et al.* [10] (see appendix B) to write the many-body density matrix as a product of high-temperature two-body density matrices. [23] The pair Coulomb density matrix was determined using the results of Pollock [53] even if these could be improved using the results of Vieillefosse. [54, 55] This procedure comes with an error that scales as $\sim \tau^3/r_s^2$ where $\tau = \beta/M$ is the *time step*, with M the number of imaginary time discretizations. A more dominant form of time step error originates from paths which cross the nodal constraint in a time less than τ . To help alleviate this effect, Brown *et al.* [10] use an image action to discourage paths from getting too close to nodes. Additional sources of error are the finite size one and the sampling error of the Monte Carlo algorithm itself. For the highest density points, statistical errors are an order of magnitude higher than time step errors.

The results at a given temperature T where obtained starting from the density matrix in the classical limit, at small thermal times, and using repetitively the *squaring* method

$$\rho_F(R_1, R_2; \beta) = \int dR' \rho_F(R_1, R'; \beta/2) \rho_F(R', R_2; \beta/2). \quad (4.23)$$

Time doubling is an improvement also because if we have accurate nodes down to a temperature T , we can do accurate simulations down to $T/2$. Eq. (4.23) is clearly symmetric in R_1 and R_2 . The time doubling cannot be repeated without reintroducing the sign problem.

Brown *et al.* [10] use $N = 33$ electrons for the fully spin polarized system and $N = 66$ electrons for the unpolarized system.

V. THE PROBLEM

We need to adopt a free fermion density matrix restriction [10] for the path integral calculation from the worm algorithm [39, 56] to the reach of the reference point in the moves ending in the Z sector: remove, close, wiggle, and displace. The worm algorithm is a particular path integral algorithm where the permutations needs not to be sampled as they are generated with the simulation evolution. We will use the primitive approximation of Eq. (A8)-(A10), randomize the reference point time slice, restrict also the G sector, in particular the advance and swap moves, choose the probability of being in the G sector, C_0 defined in Ref. [39], as small as possible, in order not to let the worm algorithm get stuck in the G sector when we have many time slices. Usually choosing a smaller time step allows to use a larger C_0 since the path is smoother and the restriction gives less problems in the transition from the G to the Z sector. Or equivalently increasing the number of time slices at fixed C_0 gives a larger permanence in the Z sector. The algorithm chooses autonomously the optimal τ to be used.

The restriction implementation is rather simple: we just reject the move whenever the proposed path is such that the ideal fermion density matrix calculated between the reference point and any of the time slices subject to newly generated particles positions has a negative value. Our algorithm is described in detail in the following section.

The trial density matrix used to perform the restriction of the fixed nodes path integral is chosen as the one of ideal fermions which is given by

$$\rho_0(R, R'; t) \propto \mathcal{A} \left[e^{-\frac{(r_i - r'_j)^2}{4\lambda t}} \right], \quad (5.1)$$

where $\lambda = \hbar^2/2m$ and \mathcal{A} is the antisymmetrization operator acting on the same spin groups of particles. We expect this approximation to be best at high temperatures and low densities when the correlation effects are weak. Clearly in a simulation of the ideal gas ($V = 0$) this restriction returns the exact result for fermions.

We will use the primitive approximation in a grand canonical ensemble calculation at fixed chemical potential μ , volume Ω , and temperature T . Decreasing the chemical potential the average number of particles diminishes. Decreasing C_0 the simulation spends more time in the Z sector.

So, we will take the Bohr radius a_0 as units of length and energies in Rydberg's units. In particular in the grand canonical simulation the path integral time step τ (Ry^{-1}) will be independent from r_s , unlike the simulations of Brown *et al.* [10]

The Coulomb potential is treated through the method of Natoli and Ceperley [57] which cures its long range nature (see Appendix C). Even if the comparison with the direct method by Fraser *et al.* [58] gives already reasonable results.

We will explicitly determine the dependence of the Jellium properties (structural and thermodynamic) on the polarization ξ .

VI. OUR ALGORITHM

Our algorithm briefly presented in the previous section is based on the worm algorithm of Boninsegni *et al.* [39, 56, 59–61]. This algorithm uses a menu of 9 moves. 3 self-complementary: swap, displace, and wiggle, and the other 6 are 3 couples of complementary moves: insert-remove, open-close, and advance-recede. These moves act on “worms” with an head *Ira* and a tail *Masha* in the β -periodic imaginary thermal time, which can swap a portion of their bodies (swap move), can move forward and backward (advance-recede moves), can be subdivided in two or joined into a bigger one (open-close moves), and can be born or die (insert-remove moves) since we are working in the grand-canonical ensemble. The configuration space of the worms is called the G sector. When the worms recombine to form a closed path we enter the so called Z sector and the path can translate in space (displace move) and can propagate in space through the bisection algorithm (wiggle move) carefully explained in Ref. [23].

In order to reach a restricted path integral we restrict the moves that end in the Z sector, that is: displace, wiggle, close, and remove. This is pictorially shown in Fig. 2 for the first three moves. It is important to stress the fact that we choose the reference point time slice randomly (i.e. we choose an integer random number between 1 and M , say m , and the reference point will then be $R_0 = R_{m\tau}$), before each move, to increase the acceptances in the

restrictions. This is allowed because we are free to perform a translation in the β -periodic imaginary thermal time. The reaches of different reference points will in general be different. In the figure the reach is schematically represented as a double cone. In order to increase

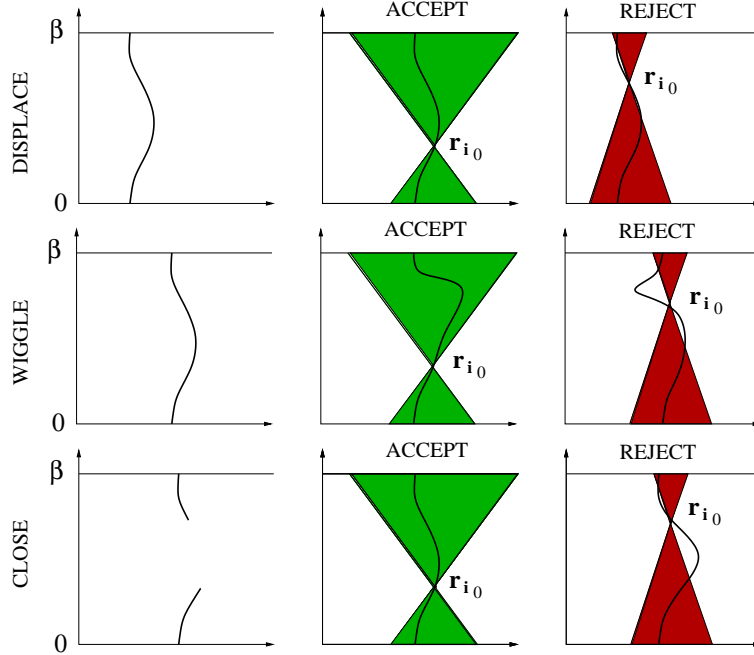


FIG. 2. (color online) Illustration of the rejection algorithm within the worm algorithm. The bold line represents schematically the closed path or the open worm, of a single electron. In the most general case these will wind through the beta periodic imaginary thermal time circle, but this is not shown in the illustration. The reference point is \mathbf{r}_{i_0} and the microscopic reach is represented schematically as the shaded doubly cylindrical region. In general the reach will be a complicated region of space-time as pointed out in Fig. 1 for the macroscopic reach. Only the three moves: displace ($Z \rightarrow Z$), wiggle ($Z \rightarrow Z$), and close ($G \rightarrow Z$) are shown. On the left we have the starting configuration and on the right we show two different actions of each move, one accepted and one rejected.

the acceptances in the restrictions we also restricted some moves in the G sector: swap and advance.

In order to implement the restriction we reject the move whenever the proposed path is such that the ideal fermion density matrix of Eq. (5.1) calculated between the reference point and any of the time slices subject to newly generated particles positions has a negative

value. That is, whenever the path ends up in a region not belonging to the reach of the reference point as shown in Fig. 2. The restriction of the G sector moves acts in the same way but on worms rather than on closed paths. When calculating diagonal properties we consider only the density matrix at the reference point.

Since the averages are only taken during the permanence in the Z sector it is fundamental to restrict the moves that end in the Z sector. Since these are the ones that have an influence on the measures of the various estimators during the run. If we enter the Z sector in such a way that we are out of the reach of the reference point the algorithm will continue wandering in the G sector till a door to the Z sector opens up. The code without restrictions gives the bosonic calculation so we are free to restrict also the G sector in order to increase the acceptances of the Z sector.

For each move we can decide the frequency of the move and the maximum number of time slices it operates on, apart from the displace move where instead of the maximum number of time slices we can decide the maximum extent of the spatial translation displacement. It is well known that Monte Carlo algorithms works better as long as we have a longer moves menu, unless of course one violates detailed balance. So the worm algorithm is very efficient in exploring all the electrons path configuration with all the necessary exchanges.

VII. RESULTS

In order to test the validity of the restriction procedure we first simulated a system of free ($V = 0$) particles without the restriction (bosons) and with the restriction (fermions). The result for the radial distribution function is shown in Fig. 3. The small discrepancy with the analytic result of Bosse *et al.* [62] is due to the finite size effect. The average number of particles in the simulation for the bosons being around 107 and for the fermions 46 for $\beta = 1 \text{ Ry}^{-1}$, 27 for $\beta = 10 \text{ Ry}^{-1}$, and 21 for $\beta = 30 \text{ Ry}^{-1}$. For the free particles we do not have any source of error coming from the imaginary time discretization. Since we were not interested in a quantitative accurate analysis we chose the simulations at smaller temperatures shorter. The volume was kept fixed at $\Omega = 1.25 \times 10^5 a_0^3$ corresponding to a half box side of $L/2 = 25a_0$. We used 20 time slices for the boson case and 80 for the fermion cases. In these simulations we find good agreement with the exact analytic results also for the internal energy per particle (kinetic and potential) and for the pressure.

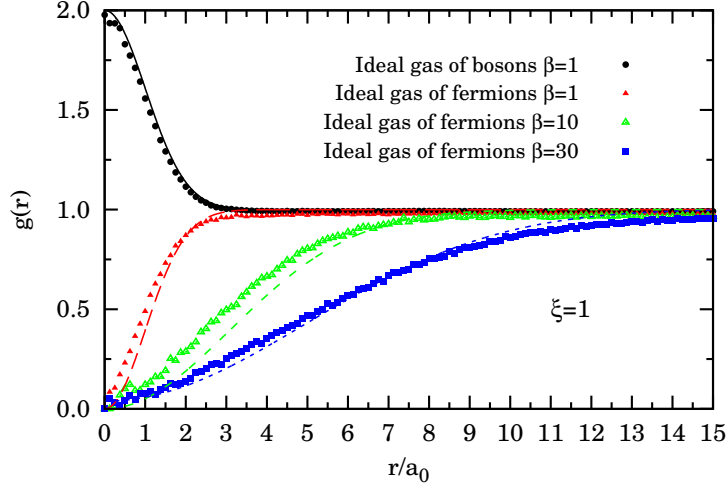


FIG. 3. (color online) The radial distribution function for an ideal gas of bosons at one inverse temperature ($\beta = 1 \text{ Ry}^{-1}$) and an ideal gas of fermions at three inverse temperatures ($\beta = 1 \text{ Ry}^{-1}, 10 \text{ Ry}^{-1}, 30 \text{ Ry}^{-1}$). We simulate fully polarized ($\xi = 1$) particles. The exact analytical results are shown as guiding lines and were derived from the work of Bosse *et al.*. [62]

Then we simulated the Jellium using for the potential energy, V , the image potential, V_I , of Eq. (C10) where we chose the short and long range splitting, necessary for the bare Coulomb potential $v(r) = 2 \text{ Ry}/r$, using the optimized method of Natoli and Ceperley [57] with an eight-order polynomial for the radial interpolation. In the long range part we keep up to 128 Fourier components.

In Table I we present our results for various thermodynamic quantities. Our results cannot be directly compared with the ones of Brown *et al.* [10] since we are running at fixed chemical potential but we believe that we are able to extend their results at higher density $r_s < 1$. Benchmark data can be found in Refs. [63, 64]. We leave a careful comparison in a subsequent work.

In Fig. 4 we show our results for the radial distribution function for the states of Table I.

TABLE I. Thermodynamic results in our simulations: β (Ry^{-1}) inverse temperature, e_k (Ry) kinetic energy per particle, e_p (Ry) potential energy per particle, P (Ry/a_0^3) pressure.

| M | ξ | \bar{N} | L | β | r_s | Θ | Γ | e_k | e_p | P |
|-----|-------|-----------|-----|---------|-------|----------|----------|----------|-------------|-------------------------|
| 60 | 1 | 35.35(4) | 5 | 0.04 | 0.945 | 3.819 | 0.085 | 31.5(5) | -0.736(3) | 5.7(1) |
| 80 | 0.154 | 57.0(2) | 50 | 4 | 8.060 | 4.180 | 0.993 | 0.365(8) | -0.0921(4) | $5.2(2) \times 10^{-5}$ |
| 680 | 1 | 30.15(3) | 50 | 68 | 9.966 | 0.250 | 13.647 | 0.016(1) | -0.12198(5) | ≈ 0 |

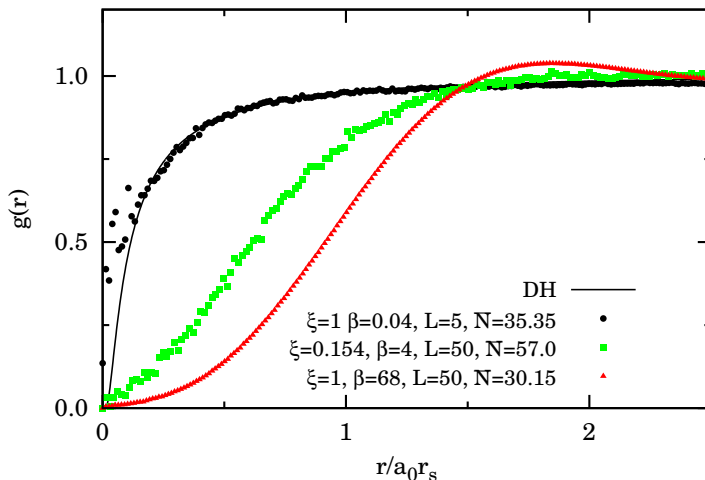


FIG. 4. (color online) The radial distribution function for Jellium in the states of Table I. Also shown is the DH result for the highest temperature state, $g_{DH}(r) = \exp \left[-\frac{\Gamma}{r} \exp \left(-\sqrt{3\Gamma} r \right) \right]$.

VIII. CONCLUSIONS

We have successfully implemented the ideal fermion density matrix restriction on the path integral worm algorithm which is able to generate the necessary permutations during the simulation evolution without the need of their explicit sampling. This allowed us to reach the fermionic finite temperature properties of a given fluid of particles interacting through a pair potential. We worked in the grand canonical ensemble and applied our method to the Jellium fluid of Wigner. Even if our results cannot be directly compared with the previous canonical calculation of Brown *et al.* [10] (this program was already carried out in our previous work [2]) we believe that they complement them with the access to

the high density regime and with the treatment of the general polarization case. In this preliminary paper we just address the validity of our method, its accuracy will be treated in a forthcoming work.

The relevance of our study relies in the fact that our simulation method is different from both the method of Ceperley *et al.* [10, 11] who uses the fixed nodes approximation in the canonical ensemble and explicitly samples the necessary permutations, and from the one of Bonitz *et al.* [12, 14–16] who combine configuration path integral Monte Carlo and permutation blocking path integral Monte Carlo. Our method is also different from others quantum Monte Carlo methods like the one of Malone *et al.* [17] that agrees well with the one of Bonitz at high densities and the direct path integral Monte Carlo one of Filinov *et al.* [18] that agrees well with Brown at low density and moderate temperature. So our new algorithm adds to the ones already used in the quest for an optimal way to calculate the properties of the fascinating Wigner’s Jellium model at finite temperatures.

We obtained results for both the structure, the radial distribution function, and various thermodynamic quantities.

We intend to adopt this method to simulate Jellium in a curved surface [6–9] in the near future. For example the Jellium on the surface of a sphere with a Dirac magnetic monopole at the center could be used to study the quantum Hall effect [65]. We already successfully applied the present method to Jellium on the surface of a sphere [66] and to two component boson-fermion plasma on a plane [19].

Appendix A: The primitive action

In this appendix we give a brief review of the derivation of the primitive approximation given in Ref. [23]. Suppose the Hamiltonian is split into two pieces $\mathcal{H} = \mathcal{T} + \mathcal{V}$, where \mathcal{T} and \mathcal{V} are the kinetic and potential operators. Recall the exact Baker-Campbell-Hausdorff formula to expand $\exp(-\tau\mathcal{H})$ into the product $\exp(-\tau\mathcal{T})\exp(-\tau\mathcal{V})$. As $\tau \rightarrow 0$ the commutator terms which are of order higher than τ^2 become smaller than the other terms and thus can be neglected. This is known as the *primitive approximation*

$$e^{-\tau(\mathcal{T}+\mathcal{V})} \approx e^{-\tau\mathcal{T}} e^{-\tau\mathcal{V}}. \quad (\text{A1})$$

hence we can approximate the exact density matrix by product of the density matrices for \mathcal{T} and \mathcal{V} alone. One might worry that this would lead to an error as $M \rightarrow \infty$, with small

errors building up to a finite error. According to the Trotter [67] formula, one does not have to worry

$$e^{-\beta(\mathcal{T}+\mathcal{V})} = \lim_{M \rightarrow \infty} [e^{-\tau\mathcal{T}} e^{-\tau\mathcal{V}}]^M. \quad (\text{A2})$$

The Trotter formula holds if the three operators \mathcal{T} , \mathcal{V} , and $\mathcal{T} + \mathcal{V}$ are self-adjoint and make sense separately, for example, if their spectrum is bounded below. [68] This is the case for the Hamiltonian describing Jellium.

Let us now write the primitive approximation in position space

$$\rho(R_0, R_2; \tau) \approx \int dR_1 \langle R_0 | e^{-\tau\mathcal{T}} | R_1 \rangle \langle R_1 | e^{-\tau\mathcal{V}} | R_2 \rangle, \quad (\text{A3})$$

and evaluate the kinetic and potential density matrices. Since the potential operator is diagonal in the position representation, its matrix elements are trivial

$$\langle R_1 | e^{-\tau\mathcal{V}} | R_2 \rangle = e^{-\tau V(R_1)} \delta(R_2 - R_1). \quad (\text{A4})$$

The kinetic matrix can be evaluated using the eigenfunction expansion of \mathcal{T} . Consider, for example, the case of distinguishable particles in a cube of side L with periodic boundary conditions. Then the exact eigenfunctions and eigenvalues of \mathcal{T} are $L^{-3N/2} e^{iK_{\mathbf{n}}R}$ and $\lambda K_{\mathbf{n}}^2$, with $K_{\mathbf{n}} = 2\pi\mathbf{n}/L$ and \mathbf{n} a $3N$ -dimensional integer vector. We are using here dimensional units. Then

$$\langle R_0 | e^{-\tau\mathcal{T}} | R_1 \rangle = \sum_{\mathbf{n}} L^{-3N} e^{-\tau\lambda K_{\mathbf{n}}^2} e^{-iK_{\mathbf{n}}(R_0 - R_1)} \quad (\text{A5})$$

$$= (4\pi\lambda\tau)^{-3N/2} \exp\left[-\frac{(R_0 - R_1)^2}{4\lambda\tau}\right], \quad (\text{A6})$$

where $\lambda = \hbar^2/2m$. Eq. (A6) is obtained by approximating the sum by an integral. This is appropriate only if the thermal wavelength of one step is much less than the size of the box, $\lambda\tau \ll L^2$. In some special situations this condition could be violated, in which case one should use Eq. (A5) or add periodic “images” to Eq. (A6). The exact kinetic density matrix in periodic boundary conditions is a theta function, $\prod_{i=1}^{3N} \theta_3(z_i, q)$, where $z_i = \pi(R_0^i - R_1^i)/L$, R^i is the i th component of the $3N$ dimensional vector R , and $q = e^{-\lambda\tau(2\pi/L)^2}$ (see chapter 16 of Ref. [69]). Errors from ignoring the boundary conditions are $O(q)$, exponentially small at large M .

A link m is a pair of time slices (R_{m-1}, R_m) separated by a time step $\tau = \beta/M$. The action S^m of a link is defined as minus the logarithm of the exact density matrix. Then the

exact path-integral expression becomes

$$\rho(R_0, R_M; \beta) = \int dR_1 \dots dR_{M-1} \exp \left[- \sum_{m=1}^M S^m \right], \quad (\text{A7})$$

It is convenient to separate out the *kinetic action* from the rest of the action. The exact kinetic action for link m will be denoted K^m

$$K^m = \frac{3N}{2} \ln(4\pi\lambda\tau) + \frac{(R_{m-1} - R_m)^2}{4\lambda\tau}, \quad (\text{A8})$$

The *inter-action* is then defined as what is left

$$U^m = U(R_{m-1}, R_m; \tau) = S^m - K^m. \quad (\text{A9})$$

In the primitive approximation the inter-action is

$$U_1^m = \frac{\tau}{2} [V(R_{m-1}) + V(R_m)], \quad (\text{A10})$$

where we have symmetrized U_1^m with respect to R_{m-1} and R_m , since one knows that the exact density matrix is symmetric and thus the symmetrized form is more accurate.

A capital letter U refers to the total link inter-action. One should not think of the exact U as being strictly the potential action. That is true for the primitive action but, in general, is only correct in the small- τ limit. The exact U also contains kinetic contributions of higher order in τ . If a subscript is present on the inter-action, it indicates the order of approximation; the primitive approximation is only correct to order τ . No subscript implies the exact inter-action.

The *residual energy* of an approximate density matrix is defined as

$$E_A(R, R'; t) = \frac{1}{\rho_A(R, R'; t)} \left[\mathcal{H} + \frac{\partial}{\partial t} \right] \rho_A(R, R'; t). \quad (\text{A11})$$

The residual energy for an exact density matrix vanishes; it is a local measure of the error of an approximate density matrix. The Hamiltonian \mathcal{H} is a function of R ; thus the residual energy is not symmetric in R and R' .

It is useful to write the residual energy as a function of the inter-action. We find

$$E_A(R, R'; t) = V(R) - \frac{\partial U_A}{\partial t} - \frac{(R - R') \cdot \nabla U_A}{t} + \lambda \nabla^2 U_A - \lambda (\nabla U_A)^2. \quad (\text{A12})$$

The terms on the right hand side are ordered in powers of τ , keeping in mind that $U(R)$ is of order τ , and $|R - R'|$ is of order $\tau^{1/2}$. One obtains the primitive action by setting the residual energy to zero and dropping the last three terms on the right hand side.

The residual energy of the primitive approximation is

$$E_1(R, R'; t) = \frac{1}{2} [V(R) - V(R')] - \frac{1}{2} (R - R') \cdot \nabla V + \frac{\lambda t}{2} \nabla^2 V - \frac{\lambda t^2}{4} (\nabla V)^2. \quad (\text{A13})$$

With a leading error of $\sim \lambda \tau^2$.

Appendix B: The pair-product action

An often useful method to determine the many-body action is to use the exact action for two electrons. [70] To justify this approach, first assume that the potential energy can be broken into a pairwise sum of terms

$$V(R) = \sum_{i < j} v(|\mathbf{r}_i - \mathbf{r}_j|), \quad (\text{B1})$$

with $|\mathbf{r}_i - \mathbf{r}_j| = r_{ij}$. Next, apply the Feynman-Kac formula for the inter-action

$$e^{-U(R_0, R_F; \tau)} = \left\langle \exp \left[- \int_0^\tau dt V(R(t)) \right] \right\rangle_{\text{RW}}, \quad (\text{B2})$$

where the notation $\langle \dots \rangle_{\text{RW}}$ means the average over all Gaussian random walks from R_0 to R_F in a “time” τ . So that

$$e^{-U(R_0, R_F; \tau)} = \left\langle \exp \left[- \int_0^\tau dt \sum_{i < j} v(r_{ij}(t)) \right] \right\rangle_{\text{RW}} \quad (\text{B3})$$

$$= \left\langle \prod_{i < j} \exp \left[- \int_0^\tau dt v(r_{ij}(t)) \right] \right\rangle_{\text{RW}} \quad (\text{B4})$$

$$\approx \prod_{i < j} \left\langle \exp \left[- \int_0^\tau dt v(r_{ij}(t)) \right] \right\rangle_{\text{RW}} \quad (\text{B5})$$

$$= \prod_{i < j} \exp [-u_2(r_{ij}, r'_{ij}; \tau)] \quad (\text{B6})$$

$$= \exp \left[- \sum_{i < j} u_2(r_{ij}, r'_{ij}; \tau) \right] = e^{-U_2(R_0, R_F; \tau)}, \quad (\text{B7})$$

where U_2 is the *pair-product* action and u_2 is the exact action for a pair of electrons. At low temperatures the pair action approaches the solution of the two particle wave equation. The result is the pair-product or Jastrow ground-state wave function, which is the ubiquitous choice for a correlated wave function because it does such a good job of describing most ground-state correlations.

The residual energy (see Eq. (A11)) for the pair-product action is less singular than for other forms. We have that

$$u_2(r_{ij}, r'_{ij}; \tau) = -\ln \left\langle \exp \left(- \int_0^\tau dt v(r_{ij}(t)) \right) \right\rangle_{\text{RW}}, \quad (\text{B8})$$

is of order τ^2 since the two body problem can be factorized into a center-of-mass term and a term that is a function of the relative coordinates. Moreover we must have

$$\frac{\partial u_2}{\partial \tau} = v(r_{ij}(\tau)), \quad (\text{B9})$$

so that

$$\frac{\partial U_2}{\partial \tau} = V(R(\tau)), \quad (\text{B10})$$

which tells that only the last three terms on the right hand side of Eq. (A12) contribute to the residual energy. We also have

$$\nabla U_2 = \sum_i \sum_{i \neq j} \nabla_i u_2(r_{ij}, r'_{ij}; \tau), \quad (\text{B11})$$

where the indices run over the particles. So the leading error of the pair-product action is $\sim \lambda \tau^3$.

Appendix C: Long-range potentials with the Ewald image technique

Suppose the bare potential in infinite d dimensional space is $v(r)$. Let us define the Fourier transform by

$$\tilde{v}_{\mathbf{k}} = \int_{-\infty}^{\infty} d^d \mathbf{r} e^{-i\mathbf{k} \cdot \mathbf{r}} v(r). \quad (\text{C1})$$

Then its inverse is

$$v(r) = \int_{-\infty}^{\infty} \frac{d^d \mathbf{k}}{(2\pi)^d} e^{i\mathbf{k} \cdot \mathbf{r}} \tilde{v}_{\mathbf{k}}. \quad (\text{C2})$$

Now let us find the energy of a single particle interacting with an infinite rectangular lattice of another particle a distance \mathbf{r} away. To make it converge we also add a uniform background of the same density (Ω =volume) of opposite charge. Thus the “image pair-potential” is equal to

$$v_I(r) = \sum_{\mathbf{L}} v(\mathbf{r} + \mathbf{L}) - \tilde{v}_0/\Omega. \quad (\text{C3})$$

The \mathbf{L} sum is over the Bravais lattice of the simulation cell $\mathbf{L} = (m_x L_x, m_y L_y, \dots)$ where m_x, m_y, \dots range over all positive and negative integers. Converting this to k -space and using the Poisson sum formula we get

$$v_I(r) = \frac{1}{\Omega} \sum'_{\mathbf{k}} \tilde{v}_{\mathbf{k}} e^{i\mathbf{k}\cdot\mathbf{r}}, \quad (\text{C4})$$

where the prime indicates that we omit the $\mathbf{k} = 0$ term; it cancels out with the background. The \mathbf{k} -sum is over reciprocal lattice vectors of the simulation box $\mathbf{k} = (2\pi n_x/L_x, 2\pi n_y/L_y, \dots)$.

Because both sums are so poorly convergent, we make the division into k -space and r -space; taking the long-range part into k -space. We write

$$v(r) = v_s(r) + v_l(r), \quad (\text{C5})$$

where the optimal splitting is discussed in the work by Natoli and Ceperley. [57] Since Fourier transform is linear, we can also write

$$\tilde{v}_{\mathbf{k}} = \tilde{v}_{s\mathbf{k}} + \tilde{v}_{l\mathbf{k}}. \quad (\text{C6})$$

Then the image pair-potential is written as

$$v_I(r) = \sum_{\mathbf{L}} v_s(|\mathbf{r} + \mathbf{L}|) + \frac{1}{\Omega} \sum_{\mathbf{k}} \tilde{v}_{l\mathbf{k}} e^{i\mathbf{k}\cdot\mathbf{r}} - \frac{1}{\Omega} \tilde{v}_0. \quad (\text{C7})$$

Now let us work with N particles of charge q_i in a periodic box and let us compute the total potential energy of the unit cell. Particles i and j are assumed to interact with a pair-potential $q_i q_j v(r_{ij})$. The image potential energy for the N -particle system is

$$V_I = \sum_{i<j} q_i q_j v_I(r_{ij}) + \sum_i q_i^2 v_M, \quad (\text{C8})$$

where v_M is the interaction of a particle with its own images; it is a Madelung constant for particle i interacting with the perfect lattice of the simulation cell. If this term were not present, particle i would only see $N - 1$ particles in the surrounding cells instead of N . We can find its value by considering the limit as two particles get close together with the image pair-potential. Hence

$$v_M = \frac{1}{2} \lim_{r \rightarrow 0} [v_I(r) - v(r)]. \quad (\text{C9})$$

Now we substitute the split up image pair-potential and collect all the terms together

$$\begin{aligned} V_I = & \sum_{i<j} \sum_{\mathbf{L}} q_i q_j v_s(|\mathbf{r}_{ij} + \mathbf{L}|) + \frac{1}{\Omega} \sum'_{\mathbf{k}} \tilde{v}_{l\mathbf{k}} \sum_{i<j} q_i q_j e^{i\mathbf{k}\cdot\mathbf{r}_{ij}} - \\ & \frac{1}{\Omega} \sum_{i<j} \tilde{v}_{s0} q_i q_j + \sum_i q_i^2 v_M. \end{aligned} \quad (\text{C10})$$

ACKNOWLEDGMENTS

We would like to thank Saverio Moroni for several relevant discussions at S.I.S.S.A. of Trieste and David Ceperley for many e-mail exchanges which has been determinant for the realization of the new algorithm.

-
- [1] R. Fantoni, *Eur. Phys. J. B* **86**, 286 (2013).
 - [2] R. Fantoni, *Eur. Phys. J. B* **94**, 63 (2021).
 - [3] N. W. Ashcroft and N. D. Mermin, *Solid State Physics* (Harcourt, Inc., Forth Worth, 1976).
 - [4] J. P. Hansen and I. R. McDonald, *Theory of simple liquids*, 2nd ed. (Academic Press, London, 1986).
 - [5] S. L. Shapiro and S. A. Teukolsky, *Black Holes, White Dwarfs, and Neutron Stars. The Physics of Compact Objects* (John Wiley & Sons, Inc., Germany, 1983).
 - [6] R. Fantoni, B. Jancovici, and G. Téllez, *J. Stat. Phys.* **112**, 27 (2003).
 - [7] R. Fantoni and G. Téllez, *J. Stat. Phys.* **133**, 449 (2008).
 - [8] R. Fantoni, *J. Stat. Mech.* , P04015 (2012).
 - [9] R. Fantoni, *J. Stat. Mech.* , P10024 (2012).
 - [10] E. W. Brown, B. K. Clark, J. L. DuBois, and D. M. Ceperley, *Phys. Rev. Lett.* **110**, 146405 (2013).
 - [11] E. Brown, M. A. Morales, C. Pierleoni, and D. M. Ceperley, Quantum monte carlo techniques and applications for warm dense matter, in *Frontiers and Challenges in Warm Dense Matter*, edited by F. Graziani *et al.* (Springer, 2014) pp. 123–149.
 - [12] T. Schoof, M. Bonitz, A. Filinov, D. Hochstul, and J. W. Dufty, Configuration path integral monte carlo, *Contrib. Plasma. Phys.* **51**, 687 (2011).
 - [13] T. Schoof, S. Groth, J. Vorberger, and M. Bonitz, *Phys. Rev. Lett.* **115**, 130402 (2015).
 - [14] T. Dornheim, S. Groth, A. Filinov, and M. Bonitz, Permutation blocking path integral monte carlo: a highly efficient approach to the simulation of strongly degenerate non-ideal fermions, *New J. Phys.* **17**, 073017 (2015).
 - [15] T. Dornheim, S. Groth, T. Sjostrom, F. D. Malone, W. M. C. Foulkes, and M. Bonitz, *Phys. Rev. Lett.* **117**, 156403 (2016).

- [16] S. Groth, T. Dornheim, T. Sjostrom, F. D. Malone, W. M. C. Foulkes, and M. Bonitz, *Phys. Rev. Lett.* **119**, 135001 (2017).
- [17] F. D. Malone, N. S. Blunt, E. W. Brown, D. K. K. Lee, J. S. Spencer, W. M. C. Foulkes, and J. J. Shepherd, Accurate exchange-correlation energies for the warm dense electron gas, *Phys. Rev. Lett.* **117**, 115701 (2016).
- [18] V. S. Filinov, V. E. Fortov, M. Bonitz, and Z. Moldabekov, Fermionic path-integral monte carlo results for the uniform electron gas at finite temperature, *Phys. Rev. E* **91**, 033108 (2015).
- [19] R. Fantoni, *Int. J. Mod. Phys. C* **29**, 1850028 (2018).
- [20] N. H. March and M. P. Tosi, *Coulomb Liquids* (Academic Press, London, 1984).
- [21] J. Friedel, *N. Cimento Suppl.* **7**, 287 (1958).
- [22] M. J. Lighthill, *Introduction to Fourier Analysis and Generalized Functions* (Cambridge University Press, 1959) theorem 19.
- [23] D. M. Ceperley, *Rev. Mod. Phys.* **67**, 279 (1995).
- [24] J. P. Hansen, *Phys. Rev. A* **8**, 3096 (1973).
- [25] J. P. Hansen and P. Vieillefosse, *Phys. Lett.* **53A**, 187 (1975).
- [26] U. Gupta and A. K. Rajagopal, *Phys. Rev. A* **22**, 2792 (1980).
- [27] F. Perrot and M. W. C. Dharma-wardana, *Phys. Rev. A* **30**, 2619 (1984).
- [28] K. S. Singwi, M. P. Tosi, R. H. Land, and A. Sjölander, *Phys. Rev.* **176**, 589 (1968).
- [29] S. Tanaka and S. Ichimaru, *Journal of the Physical Society of Japan* **55**, 2278 (1986).
- [30] F. M. C. Perrot and M. W. C. Dharma-wardana, *Phys. Rev. B* **62**, 16536 (2000).
- [31] M. W. C. Dharma-wardana and F. Perrot, *Phys. Rev. Lett.* **84**, 959 (2000).
- [32] S. Dutta and J. Dufty, *Phys. Rev. E* **87**, 032102 (2013).
- [33] S. Groth, T. Dornheim, and M. Bonitz, Free energy of the uniform electron gas: Testing analytical models against first-principles results, *Contrib. Plasma Phys.* **57**, 137 (2017).
- [34] V. V. Karasiev, T. Sjostrom, J. Dufty, and S. Trickey, *Phys. Rev. Lett.* **112**, 076403 (2014).
- [35] V. V. Karasiev, S. B. Trickey, and J. W. Dufty, *Phys. Rev. B* **99**, 195134 (2019).
- [36] D. M. Ceperley, *J. Stat. Phys.* **63**, 1237 (1991).
- [37] D. M. Ceperley, Path integral monte carlo methods for fermions, in *Monte Carlo and Molecular Dynamics of Condensed Matter Systems*, edited by K. Binder and G. Ciccotti (Editrice Compositori, Bologna, Italy, 1996).

- [38] N. V. Prokof'ev, B. V. Svistunov, and I. S. Tupitsyn, Exact, complete, and universal continuous-time worldline monte carlo approach to the statistics of discrete quantum systems, *J. Exp. Theor. Phys.* **87**, 310 (1998).
- [39] M. Boninsegni, N. Prokof'ev, and B. Svistunov, *Phys. Rev. Lett.* **96**, 070601 (2006).
- [40] K. S. Singwi and M. P. Tosi, *Sol. State Phys.* **36**, 177 (1981).
- [41] S. Ichimaru, *Rev. Mod. Phys.* **54**, 1017 (1982).
- [42] P. A. Martin, *Rev. Mod. Phys.* **60**, 1075 (1988).
- [43] E. Wigner, *Phys. Rev.* **46**, 1002 (1934).
- [44] A. J. Leggett, *Rev. Mod. Phys.* **47**, 331 (1975).
- [45] G. F. Giuliani and G. Vignale, *Quantum Theory of the Electron Liquid* (Cambridge University Press, Cambridge, 2005).
- [46] E. L. Pollock and D. M. Ceperley, *Phys. Rev. B* **36**, 8343 (1987).
- [47] D. M. Ceperley and B. J. Alder, *Phys. Rev. Lett.* **45**, 566 (1980).
- [48] R. P. Feynman, *Phys. Rev.* **90**, 1116 (1953).
- [49] R. P. Feynman, *Phys. Rev.* **91**, 1291 (1953).
- [50] R. P. Feynman, *Phys. Rev.* **90**, 1301 (1953).
- [51] R. P. Feynman and A. R. Hibbs, *Quantum Mechanics and Path Integrals* (McGraw-Hill Publishing Company, New York, 1965) page 292-293.
- [52] N. Metropolis, A. W. Rosenbluth, M. N. Rosenbluth, A. M. Teller, and E. Teller, *J. Chem. Phys.* **1087**, 21 (1953).
- [53] E. L. Pollock, *Computer Physics Communications* **52**, 49 (1988).
- [54] P. Vieillefosse, *J. Stat. Phys.* **74**, 1195 (1994).
- [55] P. Vieillefosse, *J. Stat. Phys.* **80**, 461 (1995).
- [56] M. Boninsegni, N. V. Prokof'ev, and B. V. Svistunov, *Phys. Rev. E* **74**, 036701 (2006).
- [57] V. D. Natoli and D. M. Ceperley, An optimized method for treating long-range potentials, *J. Comput. Physics* **117**, 171 (1995).
- [58] L. M. Fraser, W. M. C. Foulkes, G. Rajagopal, R. J. Needs, S. D. Kenney, and A. J. Williamson, Finite-size effects and coulomb interactions in quantum monte carlo calculations for homogeneous systems with periodic boundary conditions, *Phys. Rev. B* **53**, 1814 (1996).
- [59] R. Fantoni and S. Moroni, *J. Chem. Phys.* **141**, 114110 (2014).
- [60] R. Fantoni, Two-phase coexistence for hydrogen-helium mixtures,

- Phys. Rev. E **92**, 012133 (2015).
- [61] R. Fantoni, Supercooled superfluids in monte carlo simulations, Eur. Phys. J. B **89**, 1 (2016).
- [62] J. Bosse, K. N. Pathak, and G. S. Singh, Phys. Rev. E **84**, 042101 (2011).
- [63] T. Dornheim, S. Groth, T. Schoof, C. Hann, and M. Bonitz, Ab initio quantum monte carlo simulations of the uniform electron gas without fixed nodes: The unpolarized case, Phys. Rev. B **93**, 205134 (2016).
- [64] S. Groth, T. Schoof, T. Dornheim, and M. Bonitz, Ab initio quantum monte carlo simulations of the uniform electron gas without fixed nodes, Phys. Rev. B **93**, 085102 (2016).
- [65] V. Melik-Alaverdian, G. Ortiz, and N. E. Bonesteel, Quantum projector method on curved manifolds, J. Stat. Phys. **104**, 449 (2001).
- [66] R. Fantoni, Int. J. Mod. Phys. C **29**, 1850064 (2018).
- [67] H. F. Trotter, Proc. Am. Math. Soc. **10**, 545 (1959).
- [68] B. Simon, *Functional integration and quantum physics* (Academic, New York, 1979).
- [69] M. Abramowitz and I. A. Stegun, *Handbook of mathematical functions* (Dover, New York, 1970).
- [70] J. A. Barker, J. Chem. Phys. **70**, 2914 (1979).